



VISUALIZATION OF THE HEAT TRANSFER ON A WING LEADING EDGE SURFACE INTERNALLY IMPINGED BY A ROW OF AIR JETS

M. IMBRIALE^c, A. IANIRO, C. MEOLA, G. CARDONE

Department of Aerospace Engineering, University of Naples Federico II, Via Claudio 21, 80125 Napoli, Italy

^cCorresponding author: Tel.: +39 081 7683389; Email: michele.imbriale@unina.it

KEYWORDS:

Main subjects: convective heat transfer

Fluid: high speed flows, impinging jets, curved flow

Visualization methods: IR Thermography, 3D Visualization;

ABSTRACT: An experimental investigation of heat transfer due to a row of air jets impinging on a concave surface is presented. In particular, the test article simulates an anti-icing device. Measurements are performed with the aid of infrared thermography applied to the heated thin foil technique. Tests are carried out by varying: the jets diameter and their mutual spacing, the impinging distance, as well Reynolds and Mach numbers. Data is analyzed by accounting for the jets inclination and the curvature of the target surface and presented in terms of Nusselt number. As main results, 3D Nusselt maps show presence of flow instability which is driven by surface curvature and jet inclination

INTRODUCTION. Jets impinging on a surface give rise to high heat transfer rate, which may be exploited in many applications for drying, heating or cooling purposes. For this reason, impinging jets have been subject matter of investigation by both scientists and technicians around the world for long time. This topic was addressed in both numerical and experimental ways entailing proliferation of scientific and technical documents (see e.g., the review by Zuckerman and Lior [1]). However, the fluid-dynamics associated with a jet issuing from a nozzle (or slot) and impinging on a surface is rather complex and is still not completely understood also because of the vast variety of parameters involved which may affect the jet fluid-dynamics owing to the specific application. The vast majority of literature is concerned with a single jet, or a multitude of jets, perpendicularly impinging on a flat surface. In some applications, such as cooling of turbine blades leading edge, or wing anti-icing devices, jets impinge on a curved surface being obviously accompanied by even more complex fluid-dynamics phenomena.

The most widely used anti-icing devices for wings and engine nacelles of commercial and corporate turbofan engine aircrafts are high-temperature bleed-air anti-icing systems, commonly called *Piccolo tubes* (see e.g. the review by Gent et al. [2]). In such devices, hot air is extracted from the compressor and blown on the inside surface of the leading edge through small holes drilled in a pipe. The aim is to supply enough energy to evaporate the impinging water on the external surface of the leading edge, to maintain the surface at a temperature above the freezing value and to liquefy impinging ice crystals. Conversely, for cooling of turbine blades leading edges the jets role it to blow cold air to remove a great amount of heat to maintain the surface temperature below critical values. Anyway, apart from the jet fluid that is hot in one case and cold in the other one, both types of applications involve jets impinging on curved surfaces and so they present some common features to be understood for a complete comprehension of jet impingement heat transfer within curved surfaces.

In particular, Gau and Chung [3] analyzed the effects of both concave and convex target surfaces with impinging jets issuing from slots for the Reynolds number in the range 6000-35000. They observed, through smoke visualization, three-dimensional counter-rotating vortices on the convex surface. Conversely, they were not able to visualize any vortex structure on the concave surface because of the centrifugal disturbing force which generates instability. Moreover, also for the concave surface, they observed an increase in heat transfer with increasing the curvature, which they ascribed to the type of instability that is generally referred to as Taylor-Görtler vortices [4-5]. These effects were further investigated by Lee et al. [6] using a round turbulent jet issuing from a long straight pipe and impinging on an hemispherical concave surface; the Reynolds number was in the range 11000-50000. A similar investigation was carried out, in the same time, by Cornaro et al. [7]. The latter authors analyzed, through smoke visualization, the behavior of a jet issuing from a straight tube and impinging on a flat, or a convex, or a concave surface for Reynolds number varying between 6000 and 20000. In particular, they ascribed the increased unsteadiness of the flow on the

concave surface to the presence of recirculation effects. They also found a strong influence of the jet-to-surface spacing. Later, Iacovides et al. [8], investigating the effect of rotation on a row of non-submerged water jets impinging on a concave surface, demonstrated the presence of the *fountain effect* (maximum local heat transfer between jets).

Fenot et al. [9] studied the heat transfer due to a row of long hot jets impinging on a concave surface and showed results in terms of Nusselt number and dimensionless adiabatic temperature (i.e., effectiveness). In particular, they found the relative curvature d/D (d and D being diameter of jet and of curved surface respectively) to have two opposite effects on the Nusselt number distribution. The first involves an overall reduction of the Nusselt number, while the second entails local enhancement of the heat transfer near the impinging zone. The work by Fenot et al. [9], carried out with the aim to simulate real conditions that are encountered in the leading edge of turbine blades applications, showed the presence of the fountain effect but failed again to show the presence of Görtler vortices.

A main problem with a jet impinging on a curved surface is certainly the impingement angle. In fact, in some applications, due to geometrical constraints, or jets mutual interference, the impingement may be oblique. It is also worth noting that the jet, even if normally directed, impinges normally only in the stagnation point, while it spreads out nearby under a certain angle; the area surrounding the stagnation point is of great concern in most cases. In this context, is worth attention the work by Tawfek [10] who was the first to address the effects of oblique impingement upon a curved (convex) surface. He observed an increasing asymmetry around the point of maximum heat transfer with the impinging angle, which has no great effects on the average heating/cooling jet performance. Later, Lee et al. [11] studied, with the liquid crystal transient method, the effects of angle impingement on heat transfer on a concave impinged surface. They observed the maximum Nusselt number to occur in the upstream direction with respect to the stagnation point and an increased displacement of such a maximum with increasing the surface angle or decreasing the nozzle-to-surface distance.

In the present study infrared thermography applied to the heated thin foil technique is used for convective heat transfer measurements on a concave surface with hole jets impinging on it for varying hole diameter, hole pitch, impinging distance, Reynolds and Mach numbers. The attention is focused to gain novel information on previously observed phenomena, such as vortical structures, for a more complete understanding of the whole phenomenon.

EXPERIMENTS. The investigation is carried out with infrared thermography (IRT) applied to the heated thin foil technique [12]; this has required specific setup and test procedure as described in the following sections. It is worth noting that the experimental apparatus is similar to that used by Meola et al. [13], but with the substantial novelty that the temperature maps are rebuilt on the object mesh grid according to Cardone et al. [14]. This involves not only a different data reduction, but primarily a geometrical calibration of the infrared camera.

TEST SETUP.

The test setup, as schematically represented in Fig. 1, is basically composed of the test article, a plenum chamber and the infrared camera. The used infrared camera is the CEDIP Jade III with cooled FPA detector (320x240 pixels) working in the 3.8–5.3 μm infrared band; the nominal sensitivity, expressed in terms of Noise Equivalent Temperature Difference, is 20 mK at 300 K. The camera is positioned to view the side opposite to jet impingement.

The test article includes the leading edge of a NACA 0012 wing profile, of chord $c = 1.50$ m, with inside a spray tube to simulate an anti-icing device. Such a profile is 0.20 m long span-wise and it is stopped at about 1/10 of the chord. The bottom side is open to facilitate discharge of exhaust gases avoiding recirculation and secondary effects. To allow measurements with an infrared camera, the leading edge section is reproduced by a thin stainless steel foil (40 μm thick) lodged inside an ad hoc fixture. More specifically, the foil is grasped by two lateral molding stainless steel plates, which perform also the function of clamps for electric contacts. Each molding plate includes an hole for positioning of the spray tube inside the cavity (see Fig.1); in particular, two replaceable flanges, which are, of course, made of insulating material, allow rapid changeover of the spray tube. To avoid any foil thermal deformation and waving, the molding plates are equipped with two settable springs that convey a positive span-wise strength to the foil. To reduce measurement errors due to reflections, the foil is coated with a thin film of high emissivity paint ($\varepsilon = 0.95$).

VISUALIZATION OF THE HEAT TRANSFER ON A WING LEADING EDGE SURFACE INTERNALLY IMPINGED BY A ROW OF AIR JETS

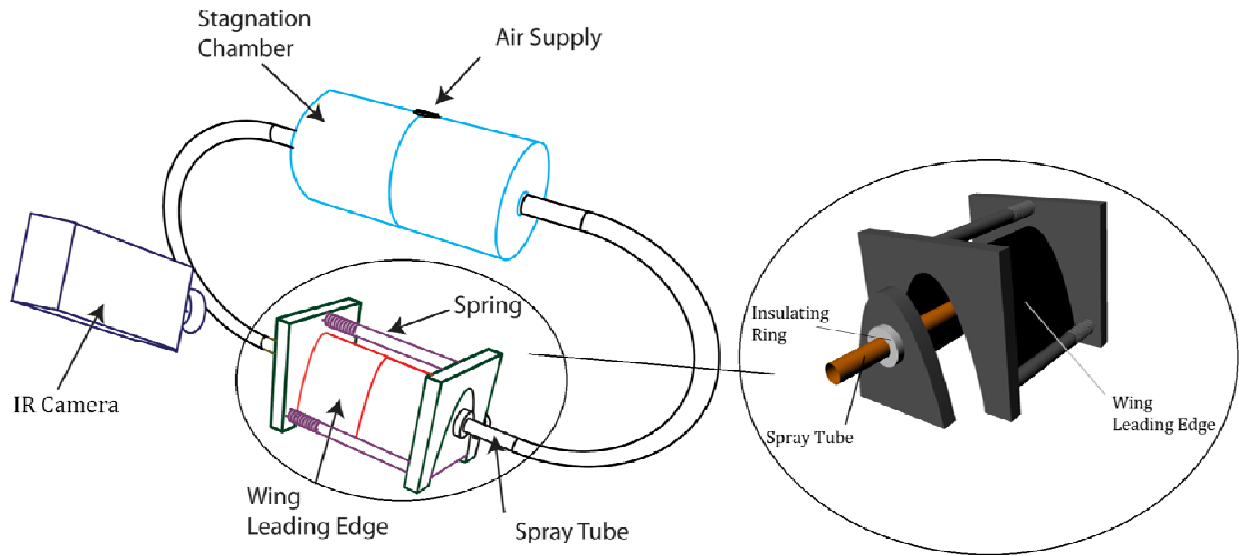


Fig. 1 Experimental Apparatus.

The spray tube, of diameter 25 mm, has a certain number of aligned holes to reproduce periodic effects of impinging jets. It is fed from both sides by air coming from the stagnation chamber, which (Fig.1) is positioned on the top. In more details, the air flow, supplied by a high pressure tank (up to 60 bar), goes through a pressure regulator valve, then to the stagnation chamber where it splits into two equal quantities to feed the spray tube from both extremities and guarantee uniform distribution of air through the tube length. Finally, air is spread out by the holes. In particular, different spray tubes are used with the number of holes varied from 3 to 5, the hole diameter d varied from 2 mm to 4 mm, and pitch on diameter ratio (the holes spacing p) varied between 5 and 15. In addition, the jet angle ϕ is varied from 0° to 50° by rotating the spray tube around its axis. The Mach number is varied from 0.6 to 1.0.

TEST PROCEDURE. As already said, heat transfer measurements are performed owing to the heated thin foil sensor for which the convective heat transfer coefficient h is given by the following relationship:

$$h = \frac{\dot{q}_j - \dot{q}_r - \dot{q}_k - \dot{q}_n}{(T_w - T_{amb})} \quad (1)$$

where \dot{q}_j is the Joule heating per unit area, \dot{q}_r is thermal radiation heat flux, \dot{q}_n is natural convection heat flux and \dot{q}_k is the foil lateral thermal conduction heat flux. T_w and T_{aw} are wall and adiabatic wall temperatures that are measured on the foil surface opposite to jets impingement (see Fig.1); (i.e., jets impinge internally on the leading edge while the infrared camera views the external surface). This is possible since the Biot number is very small ($Bi = ht / k_{steel} \approx 10^{-4}$, t and k_{steel} being the foil thickness and thermal conductivity of the foil respectively), thus the temperature can be considered instantaneously the same on both the foil sides.

By assuming the ambient as a black body at a constant temperature and the sensor surface gray in the wavelength band of interest (assumptions that can be made in this case), the net rate of radiation heat loss can be estimated as:

$$\dot{q}_r = \varepsilon \sigma (T_w^4 - T_{amb}^4) \quad (2)$$

Thermal conduction heat flux is evaluated through a Laplacian operator of temperature following Astarita and Cardone [15] and it is found to be less than 3% of the heat flux provided by Joule effect.

The natural convection heat flux \dot{q}_n can be neglected because, in the worst experimental condition (maximum temperature difference between foil and air and minimum exit Mach number), it is:

$$\frac{Gr}{Re^2} = \frac{\bar{g} \beta (T_w - T_{amb}) L}{w^2} \ll 1 \quad (3)$$

where $Gr = \bar{g} \beta (T_w - T_{amb}) L^3 / \nu^2$ is the Grashof number based on the characteristic length L equal to 10% of chord and $Re = wL / \nu$ is the Reynolds number.

To measure both wall and adiabatic wall temperatures (i.e. T_w and T_{aw}) each test run is composed of two parts. First, without electric heating, with the jets impinging and once steady state conditions are reached, a thermal image (or a sequence) is recorded that is called *cold image* and provides T_{aw} values; then, the electric current is put on and the so-called *hot image* is recorded which provides T_w values. Indeed, both T_{aw} and T_w are obtained by averaging 500 thermal images acquired in time sequence at 10 Hz; this helps filtering data from natural fluctuations phenomena. Of course, this procedure is repeated for all the test conditions which include change of the spray tube (i.e., variation of holes diameter and spacing), jet angle as well Reynolds and Mach numbers. Particular attention deserves the jet impingement inclination with respect to the chord-wise direction. This parameter may be confused with the impingement distance; however, because of the chord-wise surface curvature variation, it is more appropriate to refer to the jet angle rather than to the impingement distance.

The acquired thermal images are first analyzed in terms of temperature maps of T_{aw} and T_w and then reduced in dimensionless form in terms of the Nusselt number Nu . The influence of the most important parameters such as jet angle, jets pitch, Mach number are separately analyzed.

The Nusselt number is defined as:

$$Nu = \frac{hd}{k} \quad (4)$$

where h is the convective heat transfer coefficient defined in Eq. (1), d is the hole diameter and k is the air thermal conductivity evaluated at film temperature. It is evaluated also the Nusselt number mean distribution:

$$Nu_{mean} = \frac{1}{2p} \int_{y^*-p}^{y^*+p} Nu(x,y) dy \quad (5)$$

where y^* is the span-wise coordinate of the central jet centre and x is the chord-wise coordinate.

3D REBUILDING. Before Nusselt number calculation, the temperature maps have to be rebuilt on a 3D mesh grid from 2D IR images and the first step involves geometrical camera calibration according to the *pin-hole* camera model with an ad-hoc target. More specifically, a special support with five target tracks, called calibration target, has been designed in order to calibrate the volume occupied by the airfoil leading edge (see a scheme of the setup in Fig. 2). For every test, the calibration target is recorded in 6 positions at distance of 5 mm between them sweeping the volume of temperature measurements.

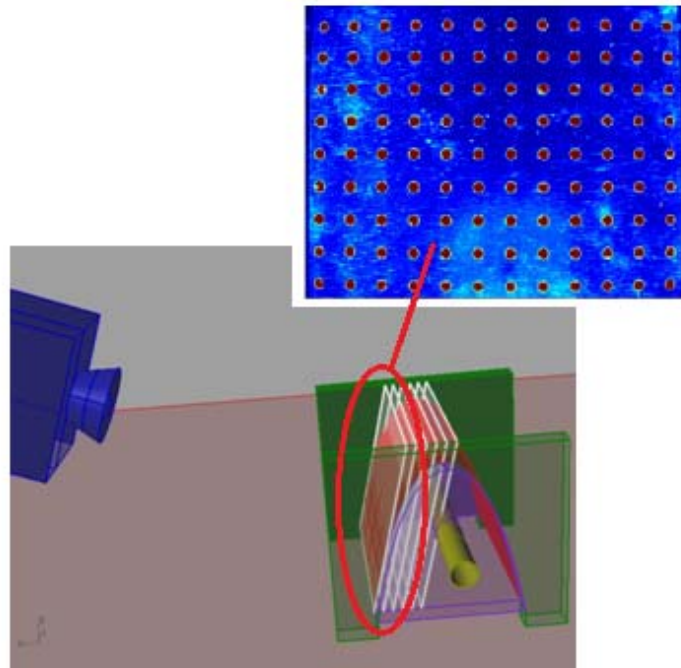


Fig. 2 Test Target. In the present picture the test target (white surface) and the profile (red surface) are shown together to better link the meaning of measurement volume. They are severally mounted between clamps.

The target is made of aluminum with regularly spaced dots on a matrix of 9x12 (see details in Fig. 2). The dots are obtained with high emissivity paint and the target is heated from its backside.

VISUALIZATION OF THE HEAT TRANSFER ON A WING LEADING EDGE SURFACE INTERNALLY IMPINGED BY A ROW OF AIR JETS

Once both the real-world coordinates of these markers and the markers positions in the image plane are known, the parameters of the camera model (that allow projection of the real-world markers in their corresponding image locations) are determined. The temperature maps are finally rebuilt on the grid (Fig. 3) representative of the observed surface by means of the camera model. In fact, the back-projection of all the points of the surface grid, with the camera model, allows obtaining, by interpolation, the measured Nusselt number values corresponding to every points. Of course, the mesh grid reproduces the NACA 0012 leading-edge region with the same spatial resolution of the IR images in order to avoid both drop of spatial resolution and increase of computational costs.

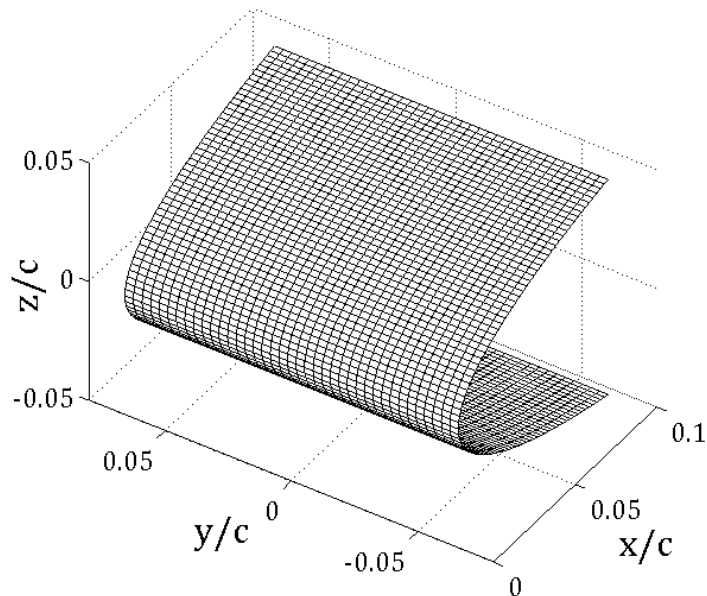


Fig. 3 3D mesh grid of the NACA-0012 leading edge.

To obtain the temperature distribution over the entire leading edge surface, at least two images must be acquired; one taken on the front-side with jets impinging on the rear (i.e., the side opposite to jets impingement) and the other one taken on the backside without any jets impingement. This obviously, entails a change of position of the infrared camera, or a 180° rotation of the leading edge profile that inevitably involves rotation of the entire test apparatus. Because of the profile symmetry, the acquisition of the two images can be simplified by taking both on the same surface by simply rotating the spray tube to comply with both of the conditions with and without jets impingement. Afterwards, the two images have to be rebuilt together on a 3D mesh grid.

RESULTS. A typical Nu map is shown in Fig 4: the jets, impinging on the leading edge, provide very high Nusselt number values in a small region with localized peaks corresponding to jet impingement. So the Nusselt number peaks clearly locate the area of jet impingement on the front-side surface of 3D rebuilding. Even though the holes are perfectly circular, the high Nu region has tendency to stretch in chord-wise direction. This behavior is due to the jets inclination with respect to the foil surface. In fact jets are perpendicular to the surface only if $\phi=0^\circ$ or $\phi=65^\circ$.

In addition, local Nusselt number maxima on the backside region are clearly visible in correspondence to the span-wise coordinate between jets. This behavior remembers the *fountain effect* found in literature (see e.g. Fenot et al. 2008). In this work, the fundamental difference is represented by the position and appearance of local maxima. In fact, a fountain effect is exactly localized between jets; while, in this case, maxima are found to be located between jets but they extend on the backside region, where jets impingement should not have great influence. Hence, what we call “*fountain like effect*” is linked to the Görtler centrifugal instability [4]. This instability is due to the surface curvature (see fig. 5) that can entail the formation of steady, stream-wise-oriented, counter-rotating vortices, which, in turn, entail heat transfer enhancement up to 100% [16].

Since jets, after impinging, are driven to be tangential to the surface, counter-rotating vortices generate a swirl component that leads to a secondary impingement on the leading edge surface. Obviously, the convective heat transfer enhances where air impinges; hence, the high Nusselt streaks on the backside region may indicate this secondary impingement. The vortices structure is spanwise periodic and, whether such hypothesis is correct, the disturbance wavelength is equal to the hole-to-hole spacing.

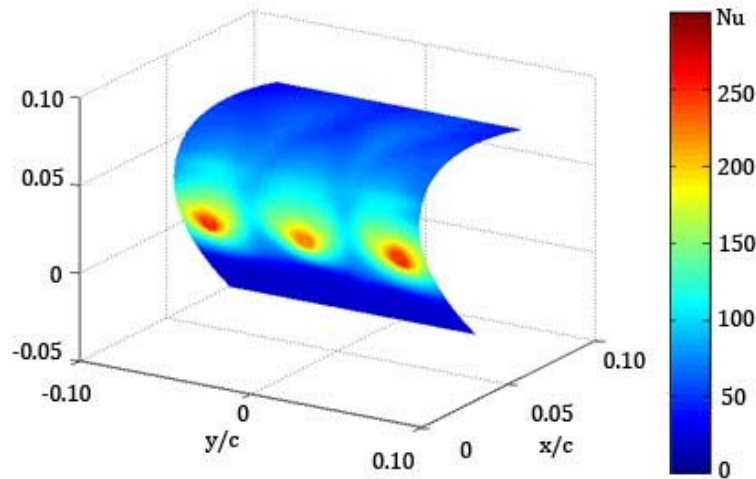


Fig. 4. Nusselt number map on a 3D mesh grid.

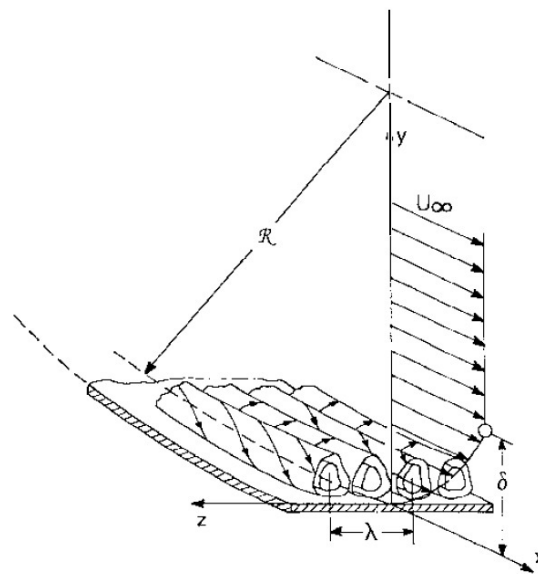


Fig. 5. Görtler Vortices (adapted from [14])

Besides, it is important to underline that high Nu streaks are visible only on one side with respect to the jets row. This behavior may be explained owing to two reasons:

- the jets inclination leads to a main flow towards the backside region;
- the Görtler instability generates vortices in case of high relative curvature.

Both hypotheses lead to a vortices generation on the backside region.

As introduced previously, some parameters are varied to evaluate their influence on the convective heat transfer and results are reported in 3D image rebuilding and in plotting data reduction. In particular, it is analyzed the influence of the following parameters: jet inclination, jet pitch and Mach number.

INFLUENCE OF JETS INCLINATION. The jets inclination (see Fig.6a) is closely linked to the nozzle-to-surface distance z , as shown in Fig.6b, with z/d the non dimensional nozzle-to-surface distance. The *piccolo tube* is positioned at 4% of the chord profile; in this configuration, the nozzle-to-surface distance increases as the jets angle decreases. Hence, the peaks of Nusselt number strengthen as the jets inclination increases from 0° to 50° (Fig.7a-e). This trend is demonstrated through the plotted Nusselt number mean distribution in Fig. 7-f. In fact, for $\phi=50^\circ$ (corresponding to the minimum value of z/d) the peak value attains its maximum. Of course, the peaks are recorded at chordwise coordinate corresponding to the row jets impingement. For jets inclination equal to 20° and 30° (when jets impinge on a surface with a high tangential component), the streaks of local Nusselt number maximum on the backside region are more evident than for other angles.

VISUALIZATION OF THE HEAT TRANSFER ON A WING LEADING EDGE SURFACE INTERNALLY IMPINGED BY A ROW OF AIR JETS

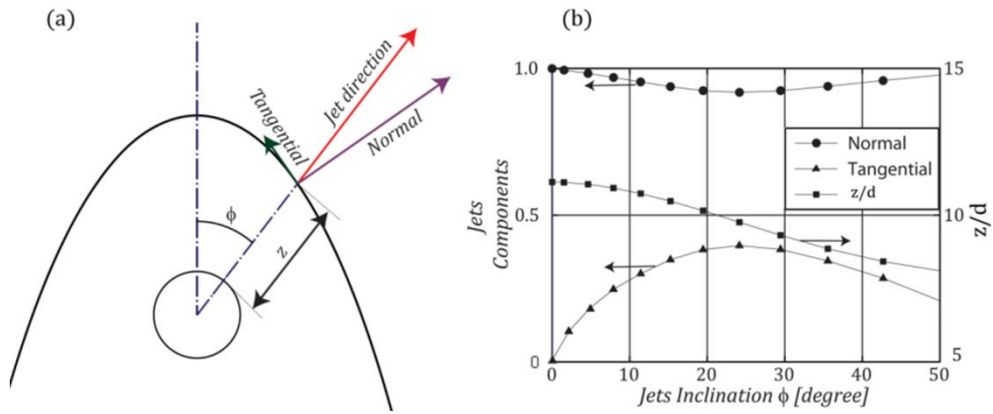


Fig. 6. Projection over leading edge surface in dependence with jets angle inclination.

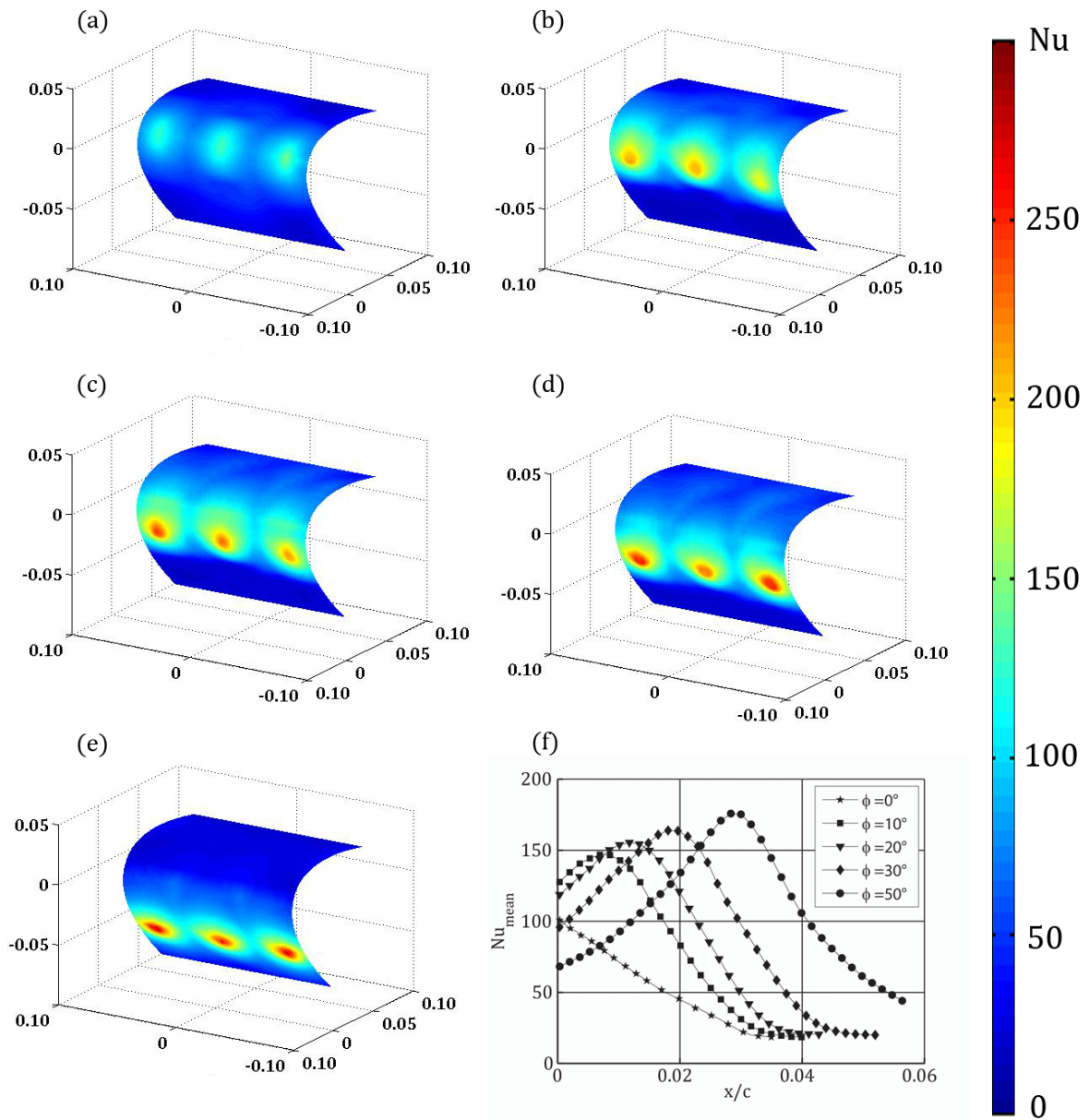


Fig. 7. Jet angle dependence on Nusselt number maps distribution for $p/d = 10$ and $M = 1.0$.

INFLUENCE OF JETS PITCH. Fig. 8 shows the Nusselt number maps for $M = 1.0$, $\phi = 50^\circ$ and pitch $p/d = 5, 10$ and 15 . The analysis of such results allows gaining information on the effects of the jet pitch in the *piccolo tube*. By varying the hole-to-hole spacing it is possible to appreciate the influence of jets interaction on convective heat transfer; it is evident that an increase of the jets pitch reduces the interaction between jets. It seems that, in the considered range, the Nu peaks are not dependent on the pitch value (Fig.9). In fact, comparing the Nu span-wise profiles plotted for different pitches values (fig. 9) the curves are practically superimposed at least in the central part. Of course, lateral jets are placed at different span-wise coordinate and are also affected by boundary effects. Contrariwise, the mean Nusselt number distributions, as shown in Fig. 8d, depend on the pitch value because, for increasing the pitch, there is a larger “valley” between two Nu peaks.

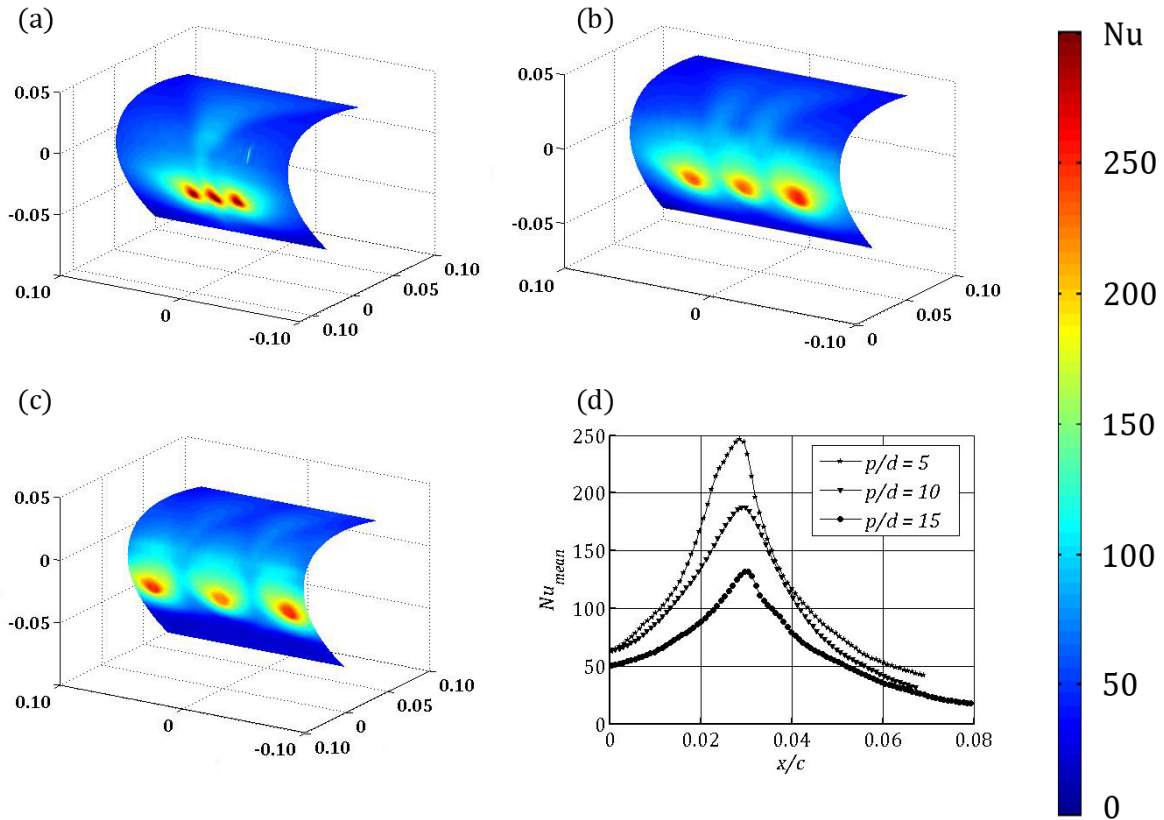


Fig. 6. Hole-to-hole spacing on Nusselt number maps for $M = 1.0$ and $\phi = 30^\circ$.

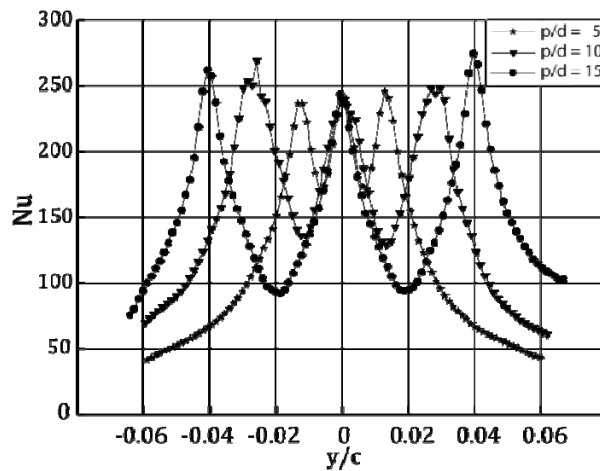


Fig. 7. Nu span-wise profiles at chord-wise coordinate equal to the impingement coordinate for $M = 1.0$ and $\phi = 30^\circ$.

VISUALIZATION OF THE HEAT TRANSFER ON A WING LEADING EDGE SURFACE INTERNALLY IMPINGED BY A ROW OF AIR JETS

With regard to the *fountain-like effect* it is important to point out that this phenomenon is dependent on the pitch value. In fact, for $p/d = 5$ (Fig.7a) the streaks of Nu maxima on the backside coalesce together giving rise to a backside Nu peak in correspondence of the central jet. So, only one couple of counter-rotating vortices develops at the smaller pitch.

INFLUENCE OF MACH NUMBER. As expected, the convective heat transfer is directly influenced by the Mach number, in particular the Nusselt number increases with Mach number increasing. In fig. 10 are shown three 3D rebuilding at different values of the Mach number (Fig.10 a-c) and a Nusselt number trend (Fig.10d) that summarizes the Mach number effect.

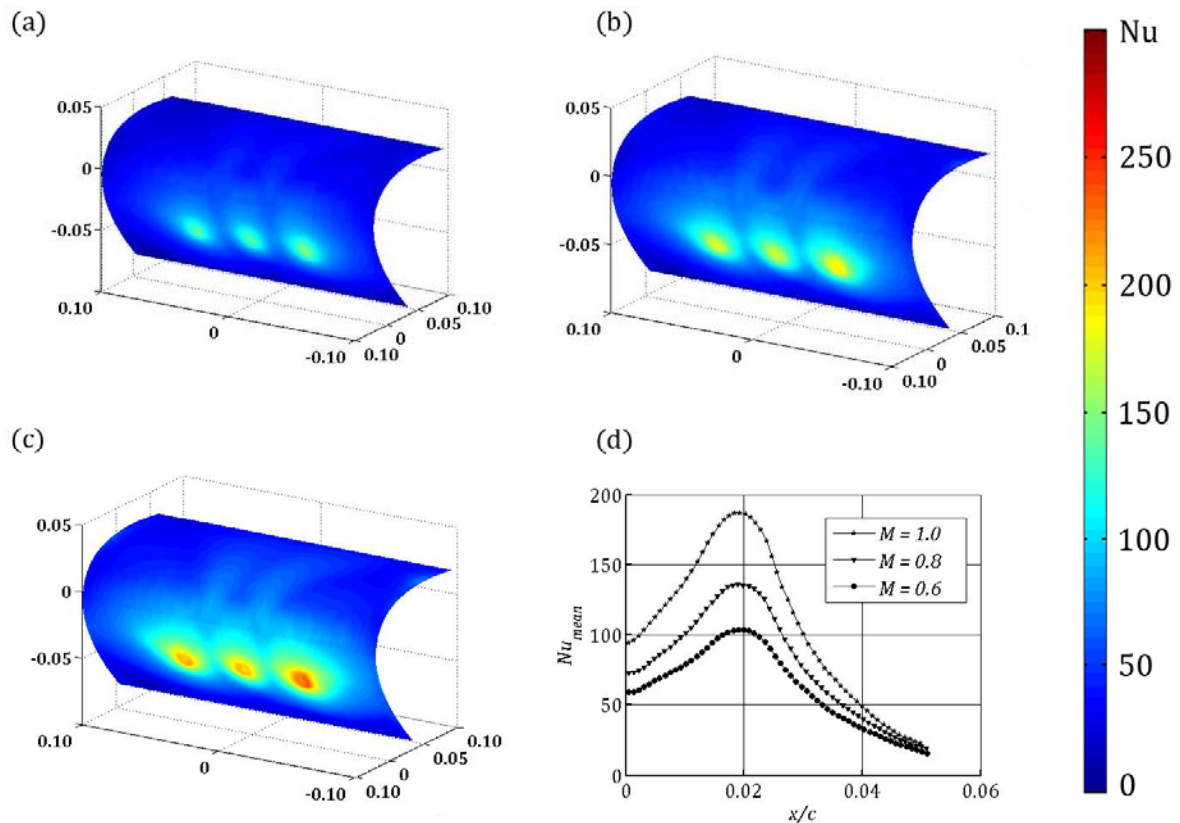


Fig. 8. Mach number dependence on Nusselt number maps distribution for $\phi = 30^\circ$ and $p/d = 10$.

CONCLUSIONS. An experimental investigation on the heat transfer by a row of jets impinging a concave surface is performed owing to a *piccolo tube* system internally impinging on a NACA 0012 wing leading edge. Heat transfer measurements are carried out with IR thermography and the heated thin foil heat transfer sensor; measurements are rebuilt in the 3D surface of the wing leading edge. The analysis of 3D images allows for a better insight in the main features of the heat transfer distribution. As main results, formation of Görtler instabilities is observed in the wall jet downstream of the jet impingement; this effect of course is enhanced with increasing the impingement angle, thus with increasing the curvature in the wall jet. In addition, the Görtler instability is driven by the jet pitch.

References

- 1 Zuckerman N. and Lior N. *Jet Impingement Heat Transfer: Physics, Correlations, and Numerical Modeling*. Advances in Heat Transfer, 2006, **39**, p. 565
2. Gent, R. W. et al. *Aircraft Icing*. Phil. Trans. R. Soc. Lond. A 2000, **358**, p. 2873
3. Gau C. and Chung C.M. *Surface Curvature Effect on Slot-Air-Jet Impingement Cooling Flow and Heat Transfer Process*. Trans. of the ASME, J. Heat Transfer 1991, **113**, p. 858
4. Saric W.S. *Görtler Vortices*. Annual Review of Fluid Mechanics 1994, **26**, p. 379

5. Floryan J.M. *Görtler instability of wall jets*. AIAA journal 1989, **27**, p. 112
6. Lee D.H. et al. *The effect of concave surface curvature on heat transfer from a fully developed round impinging jet*. IJHMT – Technical Note 1999, **42** (13), p. 2489
7. Cornaro C. et al. *Flow visualization of a round jet impinging on cylindrical surfaces*. Exp. Thermal Fluid Sci. 1999, **20**, p. 66
8. Iacovides H. et al. *Experimental study of the flow and thermal development of a row of cooling jets impinging on a rotating concave surface*. J. Turbomachinery 2005, **127**, p. 222
9. Fenot M. et al. *An experimental study on hot round jets impinging a concave surface*. Int. J. Heat and Fluid Flow 2008, **29**, p. 945
10. Tawfek A.A. *Heat Transfer Studies of the Oblique Impingement of Round Jets upon a Curved Surface*. Heat and Mass Trans. 2002, **38**, p. 467
11. Lee C.H. et al. *A study of the heat transfer characteristics of turbulent round jet impinging on an inclined concave surface using liquid crystal transient method*. Experimental Thermal and Fluid Science 2007, **31**, p. 559
12. Carlomagno G.M. and Cardone G. *Infrared thermography for convective heat transfer measurement.*, Experiments in Fluids 2010, **49**, p. 1187
13. Meola C. et al. *An experimental study of an anti-icing hot air spray-tube system*. 19th Congr. Int. Council Aeronaut. Sci.. ICAS-94-2.7.1 1994, **3**, p. 2345
14. Cardone G. et al. *Temperature maps measurements on 3D surfaces with infrared thermography*. Experiments in Fluids 2012, **52**, p. 375
15. Astarita T. and Cardone G. *Thermofluidynamic analysis of the flow in a sharp 180° turn channel*. Experimental Thermal and Fluid Science 2000, **20**, p. 188
16. McCormack P.D et al. *Taylor-Görtler Vortices and Their effect on Heat Transfer*. J. Heat Transfer 1970, **92**, p. 101